Estimating changes in source mechanisms from coda wave interferometry

David Robinson[1,2], Roel Snieder[3], and Malcolm Sambridge[1]

[1] *Research School of Earth Sciences, Australian National University, ACT, 0200, Australia*

[2] *Risk Research Group, Geoscience Australia, GPO Box 378, Canberra, 2601, Australia*

[3] *Center for Wave Phenomena and Department of Geophysics, Colorado School of Mines, Golden CO 80401, USA*

ABSTRACT

Perturbations in the source mechanism lead to variation in the coda and hence errors in separation estimates determined by coda wave interferometry. The assumption of identical source properties is a limitation of the estimates of source separation from coda wave interferometry. We show how a perturbation in the source mechanism between two identically located double couple sources can be estimated from the correlation of their coda waves measured at a single station. The mechanism perturbation, $\langle r \rangle$ is a simple function of the perturbation in dip, $\Delta\delta$ strike, $\Delta\phi_s$ and rake, $\Delta\lambda$ of the double couple. It is not possible to ascertain $\Delta\delta$, $\Delta\phi_s$ or $\Delta\lambda$ independently from the cross correlation. We validate the theory using synthetic waveforms generated from a 3D finite difference solver for the elastic wave equation.

Key words: seismic interferometry, earthquake mechanism, coda waves

1 INTRODUCTION

The waves arriving later on a seismogram arise from strong multiple scattering and are known as coda waves (Snieder, 1999). Snieder and Vrijlandt (2005) demonstrated the use of coda wave interferometry (CWI) to estimate source separation between earthquakes with identical source properties using the cross correlation of seismic waveforms measured at the same station. The normalised cross correlation given by

$$R^{(t,t_w)}(t_s) = \frac{\int_{t-t_w}^{t+t_w} u_i(t')\widetilde{u}_i(t'+t_s)dt'}{\left(\int_{t-t_w}^{t+t_w} u_i^2(t')dt' \int_{t-t_w}^{t+t_w} \widetilde{u}_i^2(t')dt'\right)^{\frac{1}{2}}} \quad (1)$$

where t_s is the shift time, measures the change between the unperturbed u_i and perturbed $\widetilde{u}_i$ displacement over a time window of length $2t_w$ (Snieder and Vrijlandt, 2005). Note that $R^{(t,t_w)}(0)$ is the correlation coefficient. Snieder (2006) demonstrates how the maximum of the normalised cross correlation over the time window t_w is related to the variance of the travel time perturbation σ_τ by

$$R_{max}^{(t,t_w)} = 1 - \frac{1}{2}\overline{\omega^2}\sigma_\tau^2 \quad (2)$$

where the square of the angular frequency $\overline{\omega^2}$ is given by

$$\overline{\omega^2} = \frac{\int_{t-t_w}^{t+t_w} \dot{u}_i^2(t')dt'}{\int_{t-t_w}^{t+t_w} u_i^2(t')dt'} \quad (3)$$

and $\dot{u}_i$ represents the derivative of u_i with respect to time, t. The relationship between the source separation δ and σ_τ is given by

$$\delta^2 = g(\alpha,\beta)\sigma_\tau^2. \quad (4)$$

Here α and β refer to P- and S-wave velocities, respectively. The function g depends on the type of excitation (explosion, point force, double couple) and on the direction of the source displacement relative to the point force or double couple. For example, for two double couple sources displaced in the fault plane, we have

$$g(\alpha,\beta) = 7\frac{\left(\frac{2}{\alpha^6} + \frac{3}{\beta^6}\right)}{\left(\frac{6}{\alpha^8} + \frac{7}{\beta^8}\right)}. \quad (5)$$

Changes in the source mechanism between two events also have an influence on the cross correlation and therefore may contaminate CWI estimates of source

separation. We derive a relationship between the perturbation of two identically located double couple source mechanisms and the cross correlation computed from their waveforms. The relationship is remarkably simple and, unlike the CWI source separation estimates, is not dependent on the frequency content of the waveforms.

To test the new expressions we use a 3D elastic wave solver to synthetically generate waveforms from gradually perturbed source mechanisms. By comparing the known source mechanism changes with estimates from the theory we are able to validate the derived relationship for small perturbations.

2 THEORY

Consider two events with different focal mechanisms located at the same hypocenter. Ignoring variation in magnitude, the waveforms measured at an arbitrary station differ in amplitude due to a change in radiation pattern associated with the perturbation of the source mechanism. There is no travel time delay for waves that follow the same scattering path due to the identical location. This latter point is the fundamental difference between this formulation and that described by Snieder and Vrijlandt (2005) for the coda wave interferometry applied to displaced source separation.

In the following we consider waves excited by a double couple source. For convenience we refer to one of the events as the unperturbed event and the second event as the perturbed event. This nomenclature recognizes that the perturbed mechanism is attained by perturbing the dip, rake and strike of the unperturbed event. The displacement associated with the unperturbed event at an arbitrary station can be computed by summing the displacement from all the scattering paths, T that reach the station

$$u_i(t) = m \sum_T u_i^{(T)}(t), \tag{6}$$

where $u_i^{(T)}$ is the component of the displacement from scattering path T in direction i normalised by the event magnitude, m. Note that the sum over all paths, T also represents a sum over wave types, P-wave and the two S-wave polarizations, for each path segment. The perturbed wave at the same station can be written as

$$\widetilde{u}_i(t) = \widetilde{m} \sum_T \widetilde{u}_i^{(T)}(t) = \widetilde{m} \sum_T (1 + r^{(T)}) u_i^{(T)}(t) \tag{7}$$

where $\widetilde{u}_i^{(T)}$ is the component of displacement from scattering path T in the i^{th} direction normalised by the event magnitude, $\widetilde{m}$ and $r^{(T)}$ measures the change in waves radiated by the source along scattering path T. Note that in deriving equation (7) we assume that the displacement cross terms associated with different scattering paths of the perturbed and un-perturbed waves sum to zero (e.g. Snieder, 2006; Snieder, 2002). In situations of strong multiple scattering the 'normalized energy' in the perturbed and unperturbed waves is the same. That is,

$$\int \sum_T u_i^{(T)2}(t')dt' = \int \sum_T (1 + r^{(T)})^2 u_i^{(T)2}(t)dt' \tag{8}$$

where the integrals are taken over the entire length of the waveform. For small perturbations and sufficiently large time windows, $2t_w$ the following approximation holds

$$\int_{t-t_w}^{t+t_w} \sum_T u_i^{(T)2}(t')dt' \approx \int_{t-t_w}^{t+t_w} \sum_T (1+r^{(T)})^2 u_i^{(T)2}(t)dt'. \tag{9}$$

The size of the time window required is dependent on the level of perturbation. The accuracy of equation (9) can be determined directly from the waveforms. The maximum cross correlation occurs when $t_s = 0$ because there is no travel time perturbation associated with a source mechanism perturbation. Substituting $t_s = 0$ and equations (6), (7) and (9) into equation (1) leads to

$$R_{max}^{(t,t_w)} = 1 + \langle r \rangle \tag{10}$$

where

$$\langle r \rangle = \frac{\sum_T r^{(T)} \int_{t-t_w}^{t+t_w} u_i^{(T)2}(t')dt'}{\sum_T \int_{t-t_w}^{t+t_w} u_i^{(T)2}(t')dt'} \tag{11}$$

is the path-weighted average of the change in displacement. The displacement, $u_i^{(T)}$ can be re-written as

$$u_i^{(T)} = s(t - t^{(T)}) f_i^{(T)}, \tag{12}$$

where $s(t - t^{(T)})$ is the source time function, $t^{(T)}$ is the travel time along trajectory T and $f_i^{(T)}$ is a radiation term associated with radiation taking off along trajectory T. The radiation term represents the amplitude and direction of the i^{th} component of the displacement, normalised by $s(t-t^{(T)})$. Assuming that the source time function, $s(t)$ is identical for each event we can re-write equation (11)

$$\langle r \rangle = \frac{\sum_T r^{(T)} f_i^{(T)2} \int_{t-t_w}^{t+t_w} s^2(t' - t^{(T)})dt'}{\sum_T f_i^{(T)2} \int_{t-t_w}^{t+t_w} s^2(t' - t^{(T)})dt'} = \frac{\sum_T r^{(T)} f_i^{(T)2}}{\sum_T f_i^{(T)2}} \tag{13}$$

and, using the fact that

$$\widetilde{u}_i^{(T)}(t) = (1 + r^{(T)}) u_i^{(T)}(t), \tag{14}$$

we obtain

$$r^{(T)} = \frac{\widetilde{f}_i^{(T)}}{f_i^{(T)}} - 1. \tag{15}$$

For elastic wave propagation we separate the radiation term, $f_i^{(T)}$ into P, SH and SV waves as follows

$$f_i^{(T)} = f_i^{(T,P)} + f_i^{(T,SV)} + f_i^{(T,SH)}, \tag{16}$$

hence

$$\langle r\rangle = \frac{\sum_T r^{(T,P)} f_i^{(T,P)2} + \sum_T r^{(T,SH)} f_i^{(T,SH)2} + \sum_T r^{(T,SV)} f_i^{(T,SV)2}}{\sum_T f_i^{(T,P)2} + \sum_T f_i^{(T,SH)2} + \sum_T f_i^{(T,SV)2}}, \tag{17}$$

where the wave types, P, SH and SV denote the wave type as it leaves the source. Replacing the summation over all paths with an angular integration over all takeoff angles yields

$$\langle r\rangle = \frac{\int \left(r^{(T,P)} f_i^{(T,P)2} + r^{(T,SH)} f_i^{(T,SH)2} + r^{(T,SV)} f_i^{(T,SV)2} \right) d\Omega}{\int f_i^{(T,P)2} d\Omega + \int f_i^{(T,SH)2} d\Omega + \int f_i^{(T,SV)2} d\Omega} \tag{18}$$

where $d\Omega = \sin\theta d\theta d\phi$, and the integration limits for $d\theta$ and $d\phi$ are $[0, 2\pi]$ and $[0, \pi]$, respectively.

We let

$$M_{jk} = M_{jk}(\phi_s, \lambda, \delta) \tag{19}$$

represent the moment tensor of the unperturbed event where ϕ_s, λ, δ indicate the strike, rake and dip, respectively. The moment tensor is related to these angles by

$$\begin{aligned}
M_{11} &= -M_o(\sin\delta\cos\lambda\sin 2\phi_s + \sin 2\delta\sin\lambda\sin^2\phi_s)\\
M_{12} = M_{21} &= M_o(\sin\delta\cos\lambda\cos 2\phi_s + \frac{1}{2}\sin 2\delta\sin\lambda\sin 2\phi_s)\\
M_{13} = M_{31} &= -M_o(\cos\delta\cos\lambda\cos\phi_s + \cos 2\delta\sin\lambda\sin\phi_s)\\
M_{22} &= M_o(\sin\delta\cos\lambda\sin 2\phi_s - \sin 2\delta\sin\lambda\cos^2\phi_s)\\
M_{23} = M_{32} &= M_o(\cos\delta\cos\lambda\sin\phi_s - \cos 2\delta\sin\lambda\cos\phi_s)\\
M_{33} &= M_o\sin 2\delta\sin\lambda,
\end{aligned} \tag{20}$$

where M_o represents the scalar moment (Kennett, 2001). The moment tensor of the perturbed event is given by $\widetilde{M}_{jk} = \widetilde{M}_{jk}(\phi_s + \Delta\phi_s, \lambda + \Delta\lambda, \delta + \Delta\delta)$, where $\Delta\phi_s$, $\Delta\lambda$ and $\Delta\delta$ represent the perturbation in strike, rake and dip, respectively. For small perturbations in these angles $\widetilde{M}_{jk}$ can be computed using a Taylor Series approximation

$$\begin{aligned}
\widetilde{M}_{jk} = M_{jk} &+ \Delta\phi_s\frac{\partial M_{jk}}{\partial\phi_s} + \Delta\lambda\frac{\partial M_{jk}}{\partial\lambda} + \Delta\delta\frac{\partial M_{jk}}{\partial\delta}\\
&+ \frac{\Delta\phi_s^2}{2}\frac{\partial^2 M_{jk}}{\partial\phi_s^2} + \frac{\Delta\lambda^2}{2}\frac{\partial^2 M_{jk}}{\partial\lambda^2} + \frac{\Delta\delta^2}{2}\frac{\partial^2 M_{jk}}{\partial\delta^2}\\
&+ \Delta\phi_s\Delta\lambda\frac{\partial^2 M_{jk}}{\partial\phi_s\partial\lambda} + \Delta\phi_s\Delta\delta\frac{\partial^2 M_{jk}}{\partial\phi_s\partial\delta}\\
&+ \Delta\lambda\Delta\delta\frac{\partial^2 M_{jk}}{\partial\lambda\partial\delta} + O(|\Delta_{angle}|^3).
\end{aligned} \tag{21}$$

From the far field approximations for the P, SV and SH displacements (e.g. Pujol, 2003)

$$and equation (12) we obtain f_i^{(P)} = \frac{1}{4\pi\rho\alpha^3 r}\hat{\boldsymbol{r}}\boldsymbol{M}\hat{\boldsymbol{r}}^T\hat{r}_i, \tag{22}$$

$$f_i^{(SV)} = \frac{1}{4\pi\rho\beta^3 r}\hat{\boldsymbol{\theta}}\boldsymbol{M}\hat{\boldsymbol{r}}^T\hat{\theta}_i, \tag{23}$$

and

$$f_i^{(SH)} = \frac{1}{4\pi\rho\beta^3 r}\hat{\boldsymbol{\phi}}\boldsymbol{M}\hat{\boldsymbol{r}}^T\hat{\phi}_i, \tag{24}$$

where ρ is the density and r is the distance. The unit vectors $\hat{\boldsymbol{r}}$, $\hat{\boldsymbol{\theta}}$ and $\hat{\boldsymbol{\phi}}$ are given by $(\sin\theta\cos\phi, \sin\theta\sin\phi, \cos\theta)$, $(\cos\theta\cos\phi, \cos\theta\sin\phi, -\sin\theta)$ and $(-\sin\phi, -\cos\phi, 0)$, respectively. Using equations (22) to (24) and integrating equation (16) over all take off angles gives

$$\int f_i^{(T)2} d\Omega = \frac{1}{4\pi\rho r}\left(\frac{16\pi}{15\alpha^6}M_o^2 + \frac{24\pi}{15\beta^6}M_o^2\right). \tag{25}$$

To derive a relationship between the source mechanism perturbation and the path-weighted average of the change in amplitude we consider a specific example. We use a coordinate system with the x-z plane aligned with the fault plane and the x-axis in the direction of the identically oriented strike and slip vectors. In that coordinate system $\delta = \pi/2$, $\lambda = 0$, $\phi_s = 0$ and equation (20) gives a moment tensor of form

$$M = \begin{pmatrix} 0 & M_o & 0\\ M_o & 0 & 0\\ 0 & 0 & 0 \end{pmatrix}. \tag{26}$$

The choice of these parameters for the moment tensor is made to simplify the derivation. However, the relationship that follows is applicable to any starting focal mechanism due to the angular integration in equation (18).

First, we consider the P waves. The P-wave contribution for scattering path T is given by equation (22) with r defined by the distance along the travel path. The P-wave contribution for the same scattering path of the perturbed wave is given by

$$\begin{aligned}
\widetilde{f}_i^{(T,P)} = \frac{1}{4\pi\rho\alpha^3 r}\Big(&\hat{\boldsymbol{r}}\boldsymbol{M}\hat{\boldsymbol{r}}^T + \Delta\phi_s\hat{\boldsymbol{r}}\frac{\partial\boldsymbol{M}}{\partial\phi_s}\hat{\boldsymbol{r}}^T + \Delta\lambda\hat{\boldsymbol{r}}\frac{\partial\boldsymbol{M}}{\partial\lambda}\hat{\boldsymbol{r}}^T\\
&+ \Delta\delta\hat{\boldsymbol{r}}\frac{\partial\boldsymbol{M}}{\partial\delta}\hat{\boldsymbol{r}}^T + \frac{\Delta\phi_s^2}{2}\hat{\boldsymbol{r}}\frac{\partial^2\boldsymbol{M}}{\partial\phi_s^2}\hat{\boldsymbol{r}}^T + \frac{\Delta\lambda^2}{2}\hat{\boldsymbol{r}}\frac{\partial^2\boldsymbol{M}}{\partial\lambda^2}\hat{\boldsymbol{r}}^T\\
&+ \frac{\Delta\delta^2}{2}\hat{\boldsymbol{r}}\frac{\partial^2\boldsymbol{M}}{\partial\delta^2}\hat{\boldsymbol{r}}^T + \Delta\phi_s\Delta\lambda\hat{\boldsymbol{r}}\frac{\partial^2\boldsymbol{M}}{\partial\phi_s\partial\lambda}\hat{\boldsymbol{r}}^T\\
&+ \Delta\phi_s\Delta\delta\hat{\boldsymbol{r}}\frac{\partial^2\boldsymbol{M}}{\partial\phi_s\partial\delta}\hat{\boldsymbol{r}}^T + \Delta\lambda\Delta\delta\hat{\boldsymbol{r}}\frac{\partial^2\boldsymbol{M}}{\partial\lambda\partial\delta}\hat{\boldsymbol{r}}^T\Big)\hat{r}_i.
\end{aligned} \tag{27}$$

Combining equations (22) and (27) with equation (15) leads to $r^{(T,P)}$, the change in P-wave displacement along scattering path T

$$\begin{aligned}
r^{(T,P)} = &\Delta\phi_s\left(\frac{-2\sin^2\theta\cos 2\phi}{\sin^2\theta\sin 2\phi}\right) + \Delta\lambda\left(\frac{-\sin 2\theta\sin\phi}{\sin^2\theta\sin 2\phi}\right)\\
&+ \Delta\delta\left(\frac{\sin 2\theta\cos\phi}{\sin^2\theta\sin 2\phi}\right) + \frac{1}{2}\Delta\phi_s^2\left(\frac{-4\sin^2\theta\sin 2\phi}{\sin^2\theta\sin 2\phi}\right)\\
&+ \frac{1}{2}\Delta\lambda^2\left(\frac{-\sin^2\theta\sin 2\phi}{\sin^2\theta\sin 2\phi}\right) + \frac{1}{2}\Delta\delta^2\left(\frac{-\sin^2\theta\sin 2\phi}{\sin^2\theta\sin 2\phi}\right)\\
&+ \Delta\phi_s\Delta\lambda\left(\frac{\sin 2\theta\cos\phi}{\sin^2\theta\sin 2\phi}\right) + \Delta\phi_s\Delta\delta\left(\frac{\sin 2\theta\sin\phi}{\sin^2\theta\sin 2\phi}\right)\\
&+ \Delta\lambda\Delta\delta\left(\frac{\sin^2\theta sin^2\phi - 2\cos^2\theta}{\sin^2\theta\sin 2\phi}\right).
\end{aligned} \tag{28}$$

Using equations (22) and (28) and integrating over the

takeoff angles leads to

$$\int r^{(T,P)} f_i^{(T,P)2} d\Omega = \frac{1}{4\pi\rho r} \frac{-8\pi M_o^2}{15\alpha^6} \left(\Delta\delta^2 + 4\Delta\phi_s^2 + \Delta\lambda^2\right). \tag{29}$$

Similarly for the SV-wave along scattering path T we obtain

$$\begin{aligned}\widetilde{f}_i^{(T,SV)} = \frac{1}{4\pi\rho\beta^3 r}\Big(&\hat{\boldsymbol{\theta}}\boldsymbol{M}\hat{\boldsymbol{r}}^T + \Delta\phi_s\hat{\boldsymbol{\theta}}\frac{\partial \boldsymbol{M}}{\partial\phi_s}\hat{\boldsymbol{r}}^T + \Delta\lambda\hat{\boldsymbol{\theta}}\frac{\partial \boldsymbol{M}}{\partial\lambda}\hat{\boldsymbol{r}}^T \\ &+ \Delta\delta\hat{\boldsymbol{\theta}}\frac{\partial \boldsymbol{M}}{\partial\delta}\hat{\boldsymbol{r}}^T + \frac{\Delta\phi_s^2}{2}\hat{\boldsymbol{\theta}}\frac{\partial^2 \boldsymbol{M}}{\partial\phi_s^2}\hat{\boldsymbol{r}}^T + \frac{\Delta\lambda^2}{2}\hat{\boldsymbol{\theta}}\frac{\partial^2 \boldsymbol{M}}{\partial\lambda^2}\hat{\boldsymbol{r}}^T \\ &+ \frac{\Delta\delta^2}{2}\hat{\boldsymbol{\theta}}\frac{\partial^2 \boldsymbol{M}}{\partial\delta^2}\hat{\boldsymbol{r}}^T + \Delta\phi_s\Delta\lambda\hat{\boldsymbol{\theta}}\frac{\partial^2 \boldsymbol{M}}{\partial\phi_s\partial\lambda}\hat{\boldsymbol{r}}^T \\ &+ \Delta\phi_s\Delta\delta\hat{\boldsymbol{\theta}}\frac{\partial^2 \boldsymbol{M}}{\partial\phi_s\partial\delta}\hat{\boldsymbol{r}}^T + \Delta\lambda\Delta\delta\hat{\boldsymbol{\theta}}\frac{\partial^2 \boldsymbol{M}}{\partial\lambda\partial\delta}\hat{\boldsymbol{r}}^T\Big)\hat{\theta}_i,\end{aligned} \tag{30}$$

hence

$$\begin{aligned}r^{(T,SV)} = &\Delta\phi_s\left(\frac{-2\sin 2\theta\cos 2\phi}{\sin 2\theta\sin 2\phi}\right) + \Delta\lambda\left(\frac{-\sin 2\phi\cos\theta}{\sin 2\theta\sin 2\phi}\right) \\ &+ \Delta\delta\left(\frac{2\cos\phi\cos 2\theta}{\sin^2\theta\sin 2\phi}\right) - 2\Delta\phi_s^2 - \frac{1}{2}\Delta\lambda^2 - \frac{1}{2}\Delta\delta^2 \\ &+ \Delta\phi_s\Delta\lambda\left(\frac{2\cos\phi\cos 2\theta}{\sin 2\theta\sin 2\phi}\right) + \Delta\phi_s\Delta\delta\left(\frac{2\sin 2\phi\cos 2\theta}{\sin 2\theta\sin 2\phi}\right) \\ &+ \Delta\lambda\Delta\delta\left(\frac{2\sin 2\theta\left(\sin^2\phi + 1\right)}{\sin 2\theta\sin 2\phi}\right)\end{aligned} \tag{31}$$

and

$$\int r^{(T,SV)} f_i^{(T,SV)2} d\Omega = \frac{1}{4\pi\rho r} \frac{-2\pi M_o^2}{15\beta^6} \left(\Delta\delta^2 + 4\Delta\phi_s^2 + \Delta\lambda^2\right). \tag{32}$$

Finally, for the SH-wave on scattering path T we get

$$\begin{aligned}\widetilde{f}_i^{(T,SH)} = \frac{1}{4\pi\rho\beta^3 r}\Big(&\hat{\boldsymbol{\phi}}\boldsymbol{M}\hat{\boldsymbol{r}}^T + \Delta\phi_s\hat{\boldsymbol{\phi}}\frac{\partial \boldsymbol{M}}{\partial\phi_s}\hat{\boldsymbol{r}}^T + \Delta\lambda\hat{\boldsymbol{\phi}}\frac{\partial \boldsymbol{M}}{\partial\lambda}\hat{\boldsymbol{r}}^T \\ &+ \Delta\delta\hat{\boldsymbol{\phi}}\frac{\partial \boldsymbol{M}}{\partial\delta}\hat{\boldsymbol{r}}^T + \frac{\Delta\phi_s^2}{2}\hat{\boldsymbol{\phi}}\frac{\partial^2 \boldsymbol{M}}{\partial\phi_s^2}\hat{\boldsymbol{r}}^T + \frac{\Delta\lambda^2}{2}\hat{\boldsymbol{\phi}}\frac{\partial^2 \boldsymbol{M}}{\partial\lambda^2}\hat{\boldsymbol{r}}^T \\ &+ \frac{\Delta\delta^2}{2}\hat{\boldsymbol{\phi}}\frac{\partial^2 \boldsymbol{M}}{\partial\delta^2}\hat{\boldsymbol{r}}^T + \Delta\phi_s\Delta\lambda\hat{\boldsymbol{\phi}}\frac{\partial^2 \boldsymbol{M}}{\partial\phi_s\partial\lambda}\hat{\boldsymbol{r}}^T \\ &+ \Delta\phi_s\Delta\delta\hat{\boldsymbol{\phi}}\frac{\partial^2 \boldsymbol{M}}{\partial\phi_s\partial\delta}\hat{\boldsymbol{r}}^T + \Delta\lambda\Delta\delta\hat{\boldsymbol{\phi}}\frac{\partial^2 \boldsymbol{M}}{\partial\lambda\partial\delta}\hat{\boldsymbol{r}}^T\Big)\hat{\phi}_i,\end{aligned} \tag{33}$$

$$\begin{aligned}r^{(T,SH)} = &\Delta\phi_s\left(\frac{2\sin\theta\sin 2\phi}{\sin\theta\cos 2\phi}\right) + \Delta\lambda\left(\frac{-\cos\phi\cos\theta}{\sin\theta\cos 2\phi}\right) \\ &+ \Delta\delta\left(\frac{-\sin\phi\cos\theta}{\sin\theta\cos 2\phi}\right) + \frac{1}{2}\Delta\phi_s^2\left(\frac{-4\sin\theta\cos 2\phi}{\sin\theta\cos 2\phi}\right) \\ &+ \frac{1}{2}\Delta\lambda^2\left(\frac{-\sin\theta\cos 2\phi}{\sin\theta\cos 2\phi}\right) + \frac{1}{2}\Delta\delta^2\left(\frac{-\sin\theta\cos 2\phi}{\sin\theta\cos 2\phi}\right) \\ &+ \Delta\phi_s\Delta\lambda\left(\frac{-\sin\phi\cos\theta}{\sin\theta\cos 2\phi}\right) + \Delta\phi_s\Delta\delta\left(\frac{\cos\phi\cos\theta}{\sin\theta\cos 2\phi}\right) \\ &+ \Delta\lambda\Delta\delta\left(\frac{\sin\theta sin^2\phi}{\sin\theta\cos 2\phi}\right)\end{aligned} \tag{34}$$

and

$$\int r^{(T,SH)} f_i^{(T,SH)2} d\Omega = \frac{1}{4\pi\rho r} \frac{-2\pi M_o^2}{3\beta^6} \left(\Delta\delta^2 + 4\Delta\phi_s^2 + \Delta\lambda^2\right). \tag{35}$$

Combining equations (25), (29), (32) and (35) with equation (18) gives

$$\langle r\rangle = -\frac{1}{2}\left(\Delta\delta^2 + 4\Delta\phi_s^2 + \Delta\lambda^2\right). \tag{36}$$

The relationship between the source mechanism perturbation and the cross correlation is then given by combining equations (10) and (36)

$$R_{max}^{(t,t_w)} = 1 - \frac{1}{2}\left(\Delta\delta^2 + 4\Delta\phi_s^2 + \Delta\lambda^2\right). \tag{37}$$

The use of non-overlapping windows to compute $R_{(max)}^{(t,t_w)}$ provides independent estimates of $\langle r\rangle$ for different center times t. These can be used to check consistency or for error analysis.

3 NUMERICAL VALIDATION

We used a finite difference (FD) solver of the 3D elastic wave equation to generate waveforms for testing the CWI source separation theory. The FD solver pmlcl3d (Olsen, 1994) was used on a Linux cluster. The solver had fourth order accuracy in space and second order accuracy in time. The model domain extended 7.68 km in each of the three dimensions. Perfectly matched absorbing layer (PML) boundary conditions (e.g. Collino and Tsogka, 2001; Marcinkovich and Olsen, 2003) were applied on the sides and bottom boundary to alleviate problems associated with reflections of the waves back towards the receiver.

The velocity of the medium was represented by a 3D Gaussian random medium with mean P-wave velocity α of 5000 ms^{-1}, standard deviation of 200 ms^{-1} and correlation length of 150 m. The medium was generated using the technique of Frankel and Clayton (1986) The S-wave velocity of the medium β was defined by

$$\beta = \frac{\alpha}{1.65} \tag{38}$$

and the density was homogeneously 2600 kgm^{-3}. The grid separation of the medium was 40 m.

$RUN0^o$ represents the unperturbed source and was created using a double couple with strike $\phi_s = 0$, dip $\delta_d = 90$, rake $\lambda = 0$ and scalar seismic moment $M_o = 1$. The source time function was created using a one-sided Gaussian pulse of form

$$s(t) = e^{\frac{-(t-a)^2}{2b^2}}, \tag{39}$$

where $a = 0.42$ s is the time lag and $b = 0.0005$ s is a measure of the width of the pulse.

$RUN5^o$ was created at the same location as $RUN0^o$ using the same $s(t)$ and a double couple source with strike $\phi_s = 5$, dip $\delta_d = 85$, rake $\lambda = 5$ and scalar seismic moment $M_o = 1$ which leads to

$$\Delta\delta_d = \Delta\phi_s = \Delta\lambda = 5^o = \frac{\pi}{36} rad \tag{40}$$

and

$$\langle r\rangle = 0.0228. \tag{41}$$

Similarly, $RUN10^o$ was created at the same location with

the same $s(t)$ using a double couple with strike $\phi_s = 10^o$, dip $\delta_d = 80^o$, rake $\lambda = 10^o$ and scalar seismic moment $M_o = 1$ which leads to

$$\Delta\delta_d = \Delta\phi_s = \Delta\lambda = 10^o = \frac{\pi}{18} rad \tag{42}$$

and

$$\langle r \rangle = 0.0914. \tag{43}$$

Figure 1 shows the displacement before and after the perturbation in the source mechanism, the correlation coefficient and $\langle r \rangle$ inferred from these waveforms. The top panel illustrates the complete waveforms. The second panel provides a more detailed illustration of the direct arrivals (left) and coda (right) for $RUN0^o$ and $RUN5^o$. The third panel illustrates the maximum cross correlation as a function of non-overlapping sliding window centroid. The bottom panel illustrates the known and correlation computed amplitude perturbation $\langle r \rangle$ in blue dashed and green solid lines, respectively, for the same non-overlapping windows. Figure 2 illustrates the CWI source perturbation estimates for the $RUN0^o$-$RUN10^o$ event pair using the same format as figure 1.

4 DISCUSSION

We derive expressions that relate a perturbation in source mechanism with the correlation coefficient and validate these with numerical simulations. The relationship between the perturbation in source mechanism and cross correlation (equation (37)) does not depend on frequency, ω. Contrastingly, when coda wave interferometry is applied to earthquake source displacement, the cross correlation does depend on ω (equation (2)). In most practical situations the source mechanism will be perturbed and displaced. The difference in dependence on frequency may hold the key to isolating the displacement, δ and the source mechanism perturbation term, $\langle r \rangle$ when applying coda wave interferometry. For example, consider two double couple sources that are both displaced and perturbed. Applying coda wave interferometry for the source displacement to the two waveforms filtered by a range of different band pass filters generates a range of R_{max} estimates. Regressing these against the dominant frequency in each band, produces a linear relationship with slope σ_τ^2 and intercept $\langle r \rangle$.

Coda wave interferometry applied to a source mechanism perturbation does not resolve the perturbation in individual angles $\Delta\phi_s$, $\Delta\delta_d$ and $\Delta\lambda$. That is, the coda wave interferometry determines the path weighted change in displacement $\langle r \rangle$ which is related to $\Delta\phi_s$, $\Delta\delta_d$ and $\Delta\lambda$ by equation (36). The true and inferred values of $\langle r \rangle$ are compared for the numerical validation. The tests work well when the the dip, strike and rake are all perturbed by 5^o (figure 1). The true value for $\langle r \rangle$ is 0.0228. If the CWI theory for source separation were misstakingly used here the estimated separation would be 8-10m. The estimates have a small bias when the dip, strike and rake are rotated by 10^o (figure 2). Note that the true value for $\langle r \rangle$ is 0.0914. If the CWI theory for source separation were used here the estimated separation would be 10-11m. The bias is not surprising since the Taylor series expansion used in the derivation is accurate for small changes in the source mechanism only. Further testing will determine when the approximations underlying the new theory break down.

The theory in this manuscript has been developed for displacement. All of the relationships hold when the displacement terms are replaced by the velocity or acceleration waveforms.

The presence of strong scattering is indicated by the strong coda in all of the synthetic waveforms. However, further tests will be used to verify that the formula is not sensitive to the properties of the medium. Further testing will also be conducted to verify whether equation (36) is sensitive to the frequency content of the source time function and to analyse the nature of the errors as a function of $\Delta\phi_s$, $\Delta\delta_d$ and $\Delta\lambda$.

5 ACKNOWLEDGEMENTS

The theory described in this manuscript was derived when David Robinson visited the Center for Wave Phenomena (CWP) at the Colorado School of Mines. The numerical validation was performed on the Terrawulf linux cluster at the Center for Advanced Data Inference, Research School of Earth Science. The Terrawulf is a 128 GNU Linux PC cluster of 2.4 GHz P4 with 1066 Mb of RAM. Peter Rickwood is thanked for his assistance with the Terrawulf. Kim Olsen is acknowledged for providing pmcl3d, the 3D finite difference solver for the elastic wave equation, and for providing advice on its use. Carlos Pacheco and John Stockwell are thanked for reviewing the manuscript. Geoscience Australia is thanked for providing the financial support for David Robinson's Ph.D.

REFERENCES

Collino, F. and C. Tsogka (2001). Application of the perfectly matched absorbing layer model to the linear elastodynamic problem in anisotropic heterogeneous media. *Geophysics* **66** (1), 294-307.

Frankel, A. and R. W. Clayton (1986). Finite difference simulations of seismic scattering: Implications for the propagation of short-period seismic waves in the crust and models of crustal heterogeneity. *Journal of Geophysical Research* **91** (B6), 6465-6489.

Kennett, B. (2001). *The seismic wavefield: Volume 1: Introduction and theoretical developments*. UK: Cambridge University Press.

Marcinkovich, C. and K. Olsen (2003). On the implementation of perfectly matched layers in a three-dimensional fourth-order velocity-stress finite difference scheme. *Journal of Geophysical Research* **B5**, 2276, doi:10.1029/2002JB002235.

Olsen, K. B. (1994). *Simulation of three-dimensional wave propagaton in the Salt Lake Basin*. Ph. D. thesis, University of Utah, Salt Lake City, Utah.

Pujol, J. (2003). *Elastic wave propagation and generation in seismology*. UK: Cambridge University Press.

Snieder, R. (1999). Imaging and averaging in complex media. In J. P. Fouque (Ed.), *Diffuse waves in complex media*, Volume 531 of *NATO Science Series C*, pp 405-454. Kluwer Academic Publishers.

Snieder, R. (2002). Coda wave interferometry and the equilibration of energy in elastic media. *Physical Review E*, **66**, 046615.

Snieder, R. (2006). The theory of coda wave interferometry. *Pure and Applied Geophysics*, **163**, 2006, pp 455-473.

Snieder, R. and M. Vrijlandt (2005). Constraining the source separation with coda wave interferometry: Theory and appication to earthquake doublets in the Hayward Fault, California. *Journal of Geophysical Research*, **110** (B04301), doi:10.1029/2004JB003317.

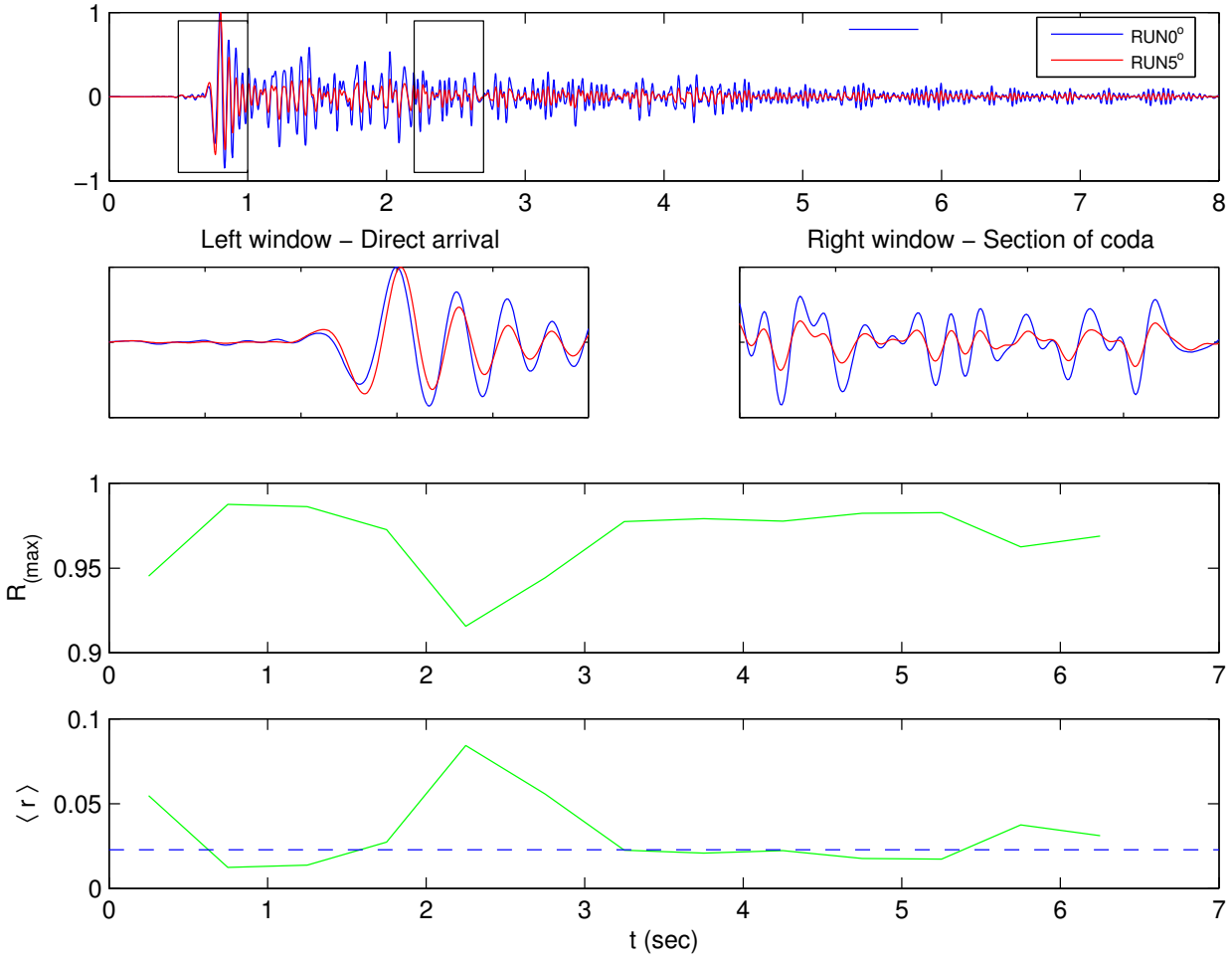

Figure 1. $RUN0^o$ and $RUN5^o$: CWI source rotation results with filtering between 1 and 5Hz. The top panel illustrates the synthetic displacement for $RUN0^o$ and $RUN5^o$ at an arbitrary recording station. The blue horizontal bar indicates the size of the time window, $2t_w$. The second panel shows the direct arrival (left) and a section of coda (right). The third panel illustrates the maximum of the cross correlation, $R_{max}^{(t,t_w)}$ for non-overlapping time windows. The final panel compares the path weighted change in displacement inferred from $R_{max}^{(t,t_w)}$ (green) with that computed from $\Delta\phi_s$, $\Delta\delta$ and $\Delta\lambda$ using equation (36) (blue dashed). Note that the true value for $\langle r \rangle$ is 0.0228. If the CWI distance formula were used here the estimated separation would be 8-10m.

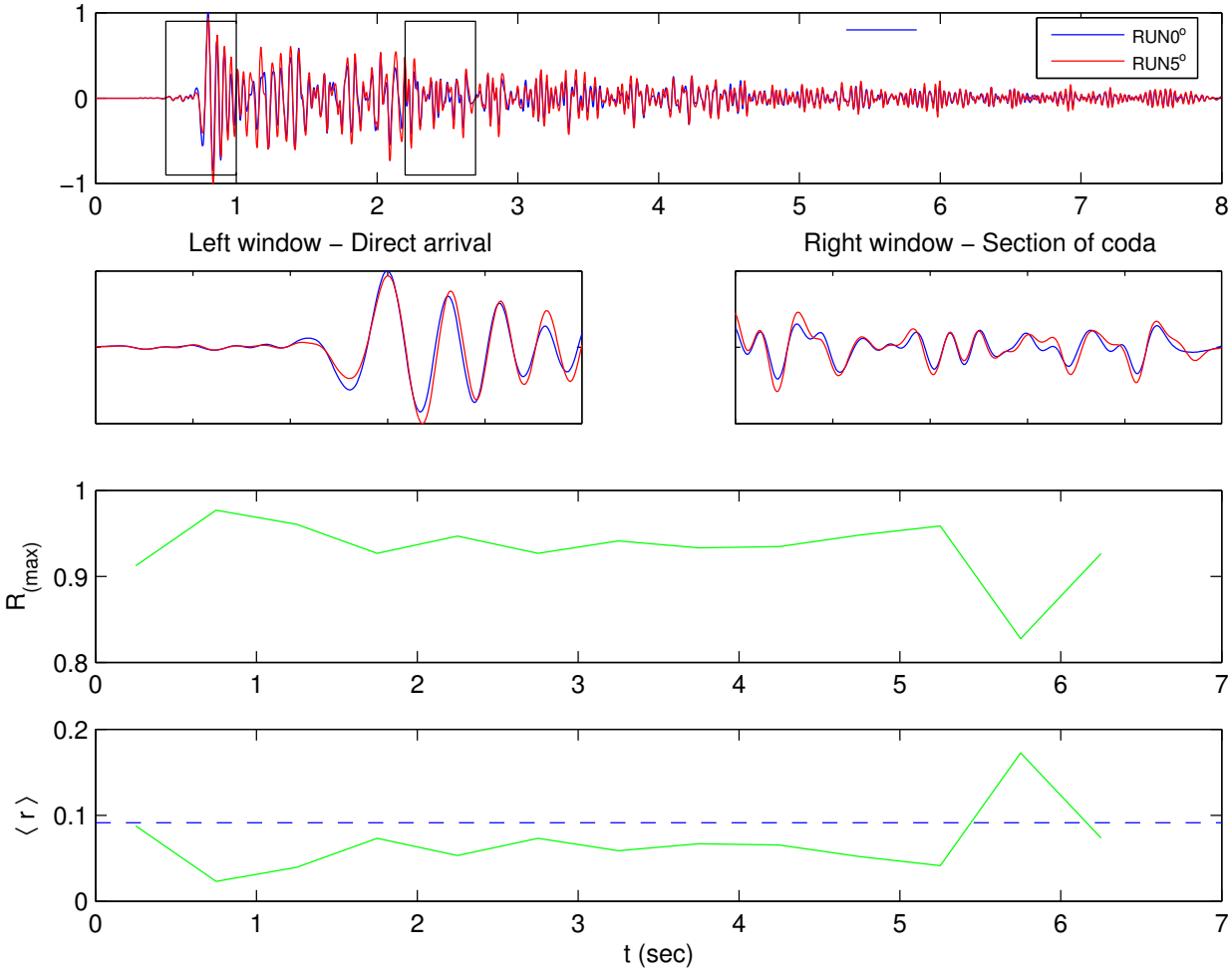

Figure 2. $RUN0^o$ and $RUN10^o$: CWI source rotation results with filtering between 1 and 5Hz, using the same format as figure 1. Note that the true value for $\langle r \rangle$ is 0.0914. If the CWI distance formula were used here the estimated separation would be 10-11m.